

Capacitor Voltage Synchronizing Control of 100% Full-Scale Wind Power Generator-Supplied Power Systems

Yang Liu, *Member IEEE, Member CSEE*

Abstract—This paper proposes a capacitor voltage synchronizing control (CVSC) system for the regulation of full-scale wind power generator-supplied power systems (FWPS). The capacitor combined with the inverter of a full-scale wind power generator (WPG) is controlled with a CVSC system to mimic the rotor dynamics of a synchronous generator (SG). WPGs are enabled to offer inertial response and primary regulation. The generation and load unbalance of a FWPS is reflected by the deviation of capacitor voltages of WPGs. Small-signal analysis was carried out to investigate the oscillatory modes of a FWPS with the CVSC system. Time-domain simulation studies were undertaken on the FWPS, and the performance of the CVSC system was studied in the cases where a load increase and a three-phase-to-ground fault occurred on the FWPS, respectively.

Index Terms—Capacitor voltage synchronizing control, full-scale wind power generator-supplied power systems.

I. INTRODUCTION

Renewable power generation has been increasing with a record-breaking speed in the last decade. By the end of 2015, there were about 433 GW of wind power and about 231 GW of solar power spinning around the globe. The annual increase of wind power and solar power installation in 2015 was 22% and 28.1%, respectively [1], [2]. Renewable power-supplied microgrids have been considered as promising prototypes for future power supply networks [3]. Renewable power sources are connected to power grids through flexibly controlled power electronics inverters [4], which introduce completely different dynamics into power grids in comparison with SGs [5]. The stability control of future renewable power-supplied power systems is the major challenge for the development of renewable power sources [6]. Considerate amount of research was carried out and the most widely investigated methods are the droop control-based strategies [7]–[14].

Frequency droop control scheme was first introduced in [7] for the control of parallel-connected inverters of ac power grids operating in the stand-alone mode. The frequency and magnitude of the inverter voltage vectors were determined with active power-frequency droop and reactive power-voltage droop characteristics, respectively. The parallel-connected inverters were controlled to mimic the load sharing behavior of conventional SGs for stable frequency and voltage of the external power grid. However, this frequency and voltage droop method has a slow and oscillating transient response [8]. As such, [8] introduced power derivative-integral terms

into the conventional frequency and voltage droop loops to improve the transient performance. Concerning the small-signal stability of such inverter-interfaced power grids with frequency droop controllers, modal analysis was undertaken in [9] and [10], the results of which revealed the relationship between the oscillatory modes of the inverter-interfaced power grids and their frequency and voltage droop loops.

To overcome the slow transient response of conventional frequency droop control methods, a phase angle droop control scheme was introduced in [11] for the control of an inverter-interfaced power grid operating in stand-alone mode. Phase angle, instead of system frequency, of the inverter voltage vector was regulated with an active power-phase angle droop characteristic to realize proper load sharing between the parallel-connected inverters. The small-signal stability of the inverter-interfaced power grids with phase angle droop controllers was studied in [12], which verified that high angle droop gains were required for proper load sharing under weak system conditions. However, high droop gains have a negative impact on the overall stability of the system. Hence, supplementary control loops were introduced in [13] for the stabilization of systems with high angle droop gains. A transient stability evaluation framework was presented in [14] for inverter-interfaced distribution systems with phase angle droop control.

For frequency droop controllers [7]–[10], they do not require any communication between inverters, which is also their most desirable feature. Regards to angle droop controllers [11]–[14], they require signals from global positioning system for angle referencing, while no communication between inverters. In contrast to the above two droop control-based strategies, centralized control [15] and master-slave control [16] schemes were proposed for the operation of inverter-interfaced power systems as well. The centralized and master-slave control schemes need communication links between inverters, thus the stability of such power grids is influenced by the reliability of the communication links.

The existing control methods [7]–[16] function on the basis of that the capacitor connected to the inverter is able to offer it enough and proper amount of energy. Therefore, most of the above works [7]–[14] have assumed that inverters are connected to ideal dc voltage sources. However, for renewable power sources, this can be hardly true without the aid of energy storages. Moreover, the beneficial dynamics of capacitors in aspects of mimicking SGs was totally ignored. The capacitors of inverters and the rotors of SGs are all energy storage

devices. A capacitor can provide inertial response like a rotor as well when load changes occur in a renewable power-supplied system. Inverters regulated by conventional droop controllers actually have blocked the inertial support from capacitors.

Instead of considering inverter interfaces only, this paper uses full-scale WPGs as the power sources of renewable power-supplied power systems. The dynamics of inverters, capacitors, and energy storages are considered in the controller design process. To realize self-synchronizing and self-load sharing, a CVSC system is proposed for the operation of a FWPS. Similar to the swing equations of SGs, voltage motion equations of capacitors are used for phase angle regulation of the inverter voltage vectors of WPGs. The capacitors of WPGs absorb or release energy in a coordinated manner with the load changes of the external power grid, such that WPGs are enabled to provide inertial response. Self-load sharing is achieved by a governor designed in the CVSC system. In contrast to the active power-frequency droop characteristic, active power-capacitor voltage droop characteristic is realized with the governor.

Compared with the centralized and master-slave control strategies [15], [16], the CVSC system does not require any communication between inverters. Different from the droop control-based methods [7]–[14], the CVSC system enables the inverter-interfaced renewable power sources to provide inertial support to the external power grid. Attributed to the CVSC system, the FWPS investigated in this paper can operate in the same manner with conventional SG-based power systems. On this basis, the off-the-shelf results on transient stability and small-signal stability of conventional power systems can be applied easily for the FWPS.

Overall, this paper is organized as follows. Section II presents a description of the FWPS investigated in this paper, as well as the design of the CVSC system. The results of the small-signal analysis of the FWPS are shown in Section III, and the oscillatory modes of the FWPS are investigated therein. Section IV illustrates the simulation results of the FWPS obtained in two different cases, where a load increase and a three-phase-to-ground fault occurred, respectively. Based on the results of small-signal analysis and time-domain simulations, conclusions are drawn in Section V, and appendices follow thereafter.

II. DESCRIPTION OF THE FWPS AND CVSC SYSTEM DESIGN

A. Description of the FWPS Investigated in This Paper

Different from the existing studies carried out on distributional-level power grids, such as [8] and [9], this paper focuses on a more general application of the CVSC system, and a FWPS with high voltage level and high generation capacity is used for analysis. It should be clarified that the CVSC proposed here is feasible in distributional power grids as well. Fig. 1 illustrates the FWPS studied in this paper, which is modified based on the Kundur four-machine two-area system [17]. The four SGs of the original system are replaced by four 889 MW wind farms, each of which is simulated

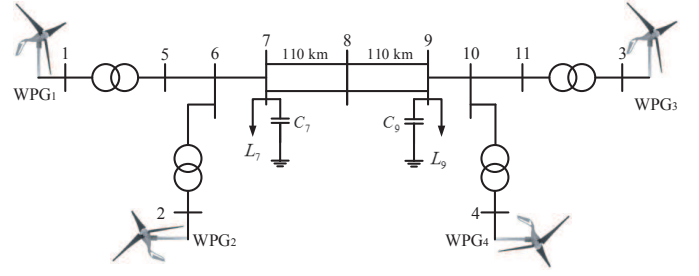


Fig. 1. Layout of the FWPS investigated in this paper.

with an aggregated model of a SG-based full-scale WPG having a 300 MW energy storage implemented respectively, as presented in Fig. 2. Energy storages are connected to the capacitors of WPGs through dc-dc converters. The parameters of transformers, loads, and transmission lines are the same as those presented in [17]. Configurations of the four WPGs are the same and their parameters are presented in Appendix B.

B. CVSC System Design

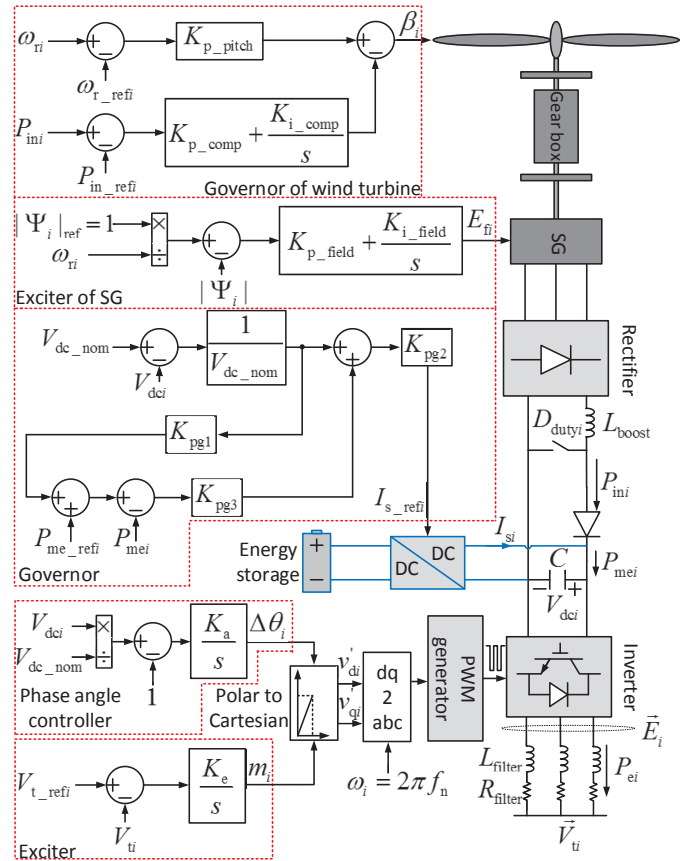


Fig. 2. The CVSC system of the i th SG-based full-scale WPG (WPG_i), where all the symbols are explained in the nomenclature presented in Appendix A.

The dynamics of the capacitor voltage of WPG_i in a FWPS can be described with

$$CV_{dci} \frac{dV_{dci}}{dt} = P_{mei} - P_{ei} \quad (1)$$

where $P_{mei} = P_{ini} + I_{si}V_{dci}$, and all the symbols shown in Fig. 2 are explained in the nomenclature of Appendix A. The

rotor speed dynamics of i th SG in a conventional n -generator power system can be described with

$$J\omega_{ri}\frac{d\omega_{ri}}{dt} = P_{mi} - P_{ei} \quad (2)$$

where ω_{ri} represents the rotor speed of i th SG, J denotes the inertia constant, P_{mi} is the mechanical power input to i th SG, and P_{ei} represents the active power output. Since the internal voltage vector of i th SG is inherently synchronous with its rotor speed, the rotational speed of its internal voltage vector follows (2) as well. Comparing (1) and (2), it can be found that capacitor voltage shows the same dynamics with rotor speed when $P_{mei} = P_{mi}$ and $C = J$ hold. Although WPG $_i$ does not have a rotating mass, WPG $_i$ can present the same dynamics with i th SG in frequency-disturbed events on condition that the rotational speed of its internal voltage vector is regulated by (1) with $P_{mei} = P_{mi}$ and $C = J$.

For this objective, the inverter control of WPG $_i$ should emulate the swing equations of i th SG. The perturbed form of the swing equations of i th SG is

$$\begin{cases} \frac{d\Delta\delta_i}{dt} = \Delta\omega_{ri} \\ \Delta\left(J\omega_{ri}\frac{d\omega_{ri}}{dt}\right) = \Delta P_{mi} - \Delta P_{ei} \end{cases} \quad (3)$$

where $\Delta\delta_i$ is the perturbed phase angle of its internal voltage vector, and $\Delta\omega_{ri}$ is the perturbed rotational speed of its internal voltage vector. Mimicking (3), the perturbed phase angle $\Delta\theta_i$ of the inverter voltage vector of WPG $_i$ should be controlled according to

$$\begin{cases} \frac{d\Delta\theta_i}{dt} = K_a\Delta V_{dci}^* \\ \Delta\left(CV_{dci}\frac{dV_{dci}}{dt}\right) = \Delta P_{mei} - \Delta P_{ei} \end{cases} \quad (4)$$

where $\Delta V_{dci}^* = (V_{dci} - V_{dc_nom})/V_{dc_nom}$, and K_a is a gain designed for better transient performance. With the phase angle controller designed based on (4), the capacitor combined with the inverter of WPG $_i$ is enabled to offer inertial support to the FWPS as i th SG in the conventional SG-based power system.

To regulate the terminal voltage of WPG $_i$, an exciter is implemented as illustrated in Fig. 2, where an integral loop is used to control the inverter modulation index m_i with the voltage error measured on the point of common coupling bus (PCCB) of WPG $_i$. The inverter voltage vector \vec{E}_i of WPG $_i$ then can be denoted as

$$\vec{E}_i = E_i\angle\theta_i = E_i\angle(\Delta\theta_i + \omega_i t) \quad (5)$$

where $\omega_i = 2\pi f_n$. Then the active power output of WPG $_i$ in a n -WPG FWPS can be written as

$$P_{ei} = E_i^2 G_{ii} + \sum_{j=1, j \neq i}^n E_i E_j [B_{ij} \sin(\Delta\theta_i - \Delta\theta_j) + G_{ij} \cos(\Delta\theta_i - \Delta\theta_j)] \quad (6)$$

where G_{ij} and B_{ij} are the real and imaginary parts of the i th row, j th column element of the admittance matrix of the

FWPS. Comparatively, the active power output of i th SG in the conventional n -SG power system is [17],

$$P_{ei} = E_i^2 G_{ii} + \sum_{j=1, j \neq i}^n E_i E_j [B_{ij} \sin(\delta_i - \delta_j) + G_{ij} \cos(\delta_i - \delta_j)] \quad (7)$$

Therefore, in the conventional SG-based power system, the stable active power output of i th SG implies that

$$\frac{d\delta_i}{dt} - \frac{d\delta_j}{dt} = \omega_i - \omega_j = 0 \quad (8)$$

where $i \neq j$. Therefore, the generation and load balance of a conventional SG-based power system is characterized by the synchronization of the rotor speed of SGs. Referring to (7), the stable active power output of WPG $_i$ implies that

$$\begin{aligned} \frac{d\Delta\theta_i}{dt} - \frac{d\Delta\theta_j}{dt} &= K_a(\Delta V_{dci}^* - \Delta V_{dcj}^*) \\ &= K_a(V_{dci}^* - V_{dcj}^*) = 0 \end{aligned} \quad (9)$$

Therefore, the generation and load balance of the FWPS is characterized by the synchronization of the capacitor voltages of WPGs on condition that $K_a \neq 0$. Synthesizing (3), (4), (8), and (9), it can be found that the internal voltage vector of a WPG with the phase angle controller moves in the same manner with that of a SG. The energy stored in the capacitor of WPG $_i$ is

$$E_{\text{capacitori}} = \frac{1}{2}CV_{dci}^2 - \frac{1}{2}CV_{dc0i}^2 = \int_0^t (P_{mei} - P_{ei})dt \quad (10)$$

where V_{dc0i} denotes the capacitor voltage of WPG $_i$ at $t = 0$ s. In the case where a load increase occurs in the FWPS, capacitors release the energy stored to provide inertial support to the FWPS. The case of load drop follows similarly.

Analogous to SG-based conventional power systems, primary regulation is needed in the FWPS for proper load sharing among WPGs. A governor is implemented for capacitor voltage control as presented in Fig. 2. The governor of a WPG controls the power flowing by the capacitor and functions after the inertial response of the capacitor. Active power-capacitor voltage droop characteristic is realized by the K_{pg1} loop in the governor. Compared with the case of conventional power systems, in which constant frequency errors exist after primary frequency regulations, there will be constant capacitor voltage errors after the primary regulation of WPGs in the FWPS.

With respect to the control of SGs and turbine blades of WPGs, a constant flux controller is employed for the excitation control of SGs, and a wind turbine governor is utilized for rotor speed and active power control of SGs, as shown in Fig. 2. To verify the stability of the FWPS in the small and in the large, small-signal and time-domain simulation studies are presented in the following sections, respectively.

III. SMALL-SIGNAL ANALYSIS OF THE FWPS

The FWPS introduced in Section II-A was linearized at: $P_{e1} = 685$ MW, $V_{t1} = 1.03\angle 0^\circ$, $P_{e2} = 665$ MW, $V_{t2} = 1.01\angle -9.43^\circ$, $P_{e3} = 700$ MW, $V_{t3} = 1.03\angle -22.52^\circ$, $P_{e4} = 650$ MW, $V_{t4} = 1.01\angle -32.68^\circ$. Eighth-order models were used for the description of the SG of WPGs [18], and

TABLE I
SYSTEM MODES OF THE RPS CONTROLLED BY CVSC SCHEME

Eigenvalues		Frequency (Hz)	Damping Ratio	Dominant States
No.	Real	Imaginary		
1,2	-9.0414	$\pm 3.7606E2$	59.8521	0.0240 Ψ_{q3}
3,4	-9.0234	$\pm 3.7598E2$	59.8388	0.0240 Ψ_{q1}
5,6	-9.0232	$\pm 3.7597E2$	59.8379	0.0240 Ψ_{q2}
7,8	-9.0277	$\pm 3.7597E2$	59.8372	0.0240 Ψ_{q4}
9	-52.9610	-	-	V_{dc1}
10	-52.7246	-	-	V_{dc3}
11	-51.6736	-	-	V_{dc2}
12	-51.6517	-	-	V_{dc4}
13,14	-5.4940	± 28.5222	4.5395	0.1891 ω_{r1}
15,16	-5.6389	± 30.7479	4.8937	0.1804 ω_{r4}
17,18	-5.6614	± 28.9264	4.6038	0.1921 ω_{r2}
19,20	-5.5174	± 29.8855	4.7564	0.1816 ω_{r3}
21	-29.9355	-	-	Ψ'_{kq1}
22	-29.3762	-	-	Ψ'_{kq2}
23	-29.5797	-	-	Ψ'_{kq3}
24	-29.0189	-	-	Ψ'_{kq4}
25	-16.1247	-	-	Ψ'_{kd1}
26	-16.6668	-	-	Ψ'_{kd4}
27	-16.3040	-	-	Ψ'_{kd2}
28	-16.4182	-	-	Ψ'_{kd3}
29,30	-0.1282	± 3.2972	0.5248	0.0388 ω_{t1}
31,32	-0.1200	± 3.3042	0.5259	0.0363 ω_{t2}
33,34	-0.1032	± 3.3433	0.5321	0.0309 ω_{t4}
35,36	-0.1124	± 3.3273	0.5296	0.0337 ω_{t3}
37	-1.3278	-	-	$\Delta\theta_4$
38	-1.3049	-	-	$\Delta\theta_2$
39	-8.9819E-13	-	-	$\Delta\theta_1$
40	-0.6776	-	-	Ψ'_{f4}
41	-0.5778	-	-	Ψ'_{f3}
42	-0.5318	-	-	Ψ'_{f2}
43,44	-0.2934	± 0.1063	0.0169	0.9402 m_2
45	-0.4442	-	-	Ψ'_{f1}
46	-0.3810	-	-	m_3
47	-0.2485	-	-	m_1
48	-0.2465	-	-	m_4

two-mass models were employed for the drive train of wind turbines [19]. The oscillatory modes of the FWPS are obtained as illustrated in Table I. It can be found that all eigenvalues of the system matrix have negative real parts. Therefore, the FWPS controlled with the CVSC system is stable in the small.

Low-frequency oscillation modes, whose frequency are ranged within 0.2-2.5 Hz, are found in the rotational speed ω_{ti} ($i = 1, 2, 3, 4$) of the wind turbine of WPGs. However, low-frequency oscillation damping is not the objective of this paper. The design of damping controllers for these low-frequency oscillatory modes has not been presented here.

The impact of control parameter K_a on the singular values of transfer function $\frac{P_{e1}}{V_{dc1}}$ is illustrated by Fig. 3. It can be observed that the active power response capability of WPGs is improved as K_a increases. In turn, the influence of high frequency noise are more significant as K_a becomes larger. Considering the tradeoff between the active power response capability and the high-frequency noise attenuation, K_a is selected as 10 in this paper. Parameters of the full-scale WPGs of the FWPS presented in Appendix B are chosen such that all the eigenvalues of the system matrix locate in the left-half complex plane.

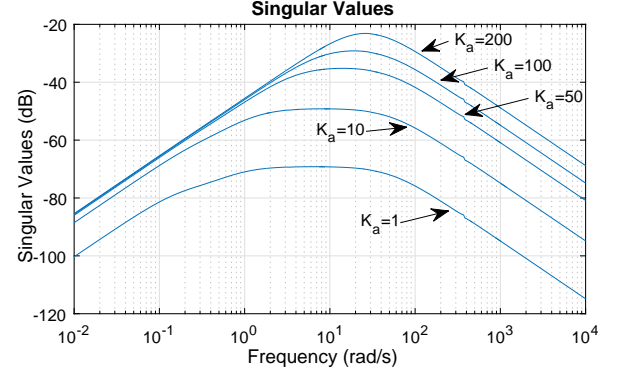


Fig. 3. Influence of K_a on the singular values of transfer function $\frac{P_{e1}(p.u.)}{V_{dc1}(V)}$.

IV. TIME-DOMAIN SIMULATION RESULTS OF THE FWPS

In order to verify the stability of the FWPS in the large, time-domain simulations considering electromagnetic transients of the system were undertaken, and the obtained results are presented in this section. In the FWPS, WPG₂ and WPG₄ are implemented with the CVSC system. WPG₃ is chosen as the slack machine, and it does not have a governor installed.

A. A 400 MW Load Increase Occurred on Load Bus 9 of the FWPS at $t = 2$ s

A 400 MW load was connected on load bus 9 at $t = 2$ s. The dynamics of WPG₄ and that of the load bus voltage are presented in Fig. 4. Due to the load increase, the magnitude of load bus voltage dropped, and the three-phase voltages measured on load bus 9 are shown in Fig. 4 (a). Meanwhile, the load current increased, which resulted in more active power output of WPG₄ as illustrated in Fig. 4 (c). This process was the inertial response from WPG₄, which was achieved by the combined effort of the capacitor and the energy storage. As depicted in Fig. 4 (g), the capacitor voltage of WPG₄ dropped due to the upsurge of its active power output. Moreover, the energy storage provided more power to the capacitor as illustrated in Fig. 4 (d). The drop of capacitor voltage also lead to the active power output increase of the SG of WPG₄, which is verified by Fig. 4 (e). In this way, the kinetic energy stored in the rotor of the SG was released to provided inertial support for the capacitor voltage drop. Besides the increase of active power generation, WPG₄ generated more reactive power to the external power grid, and a step increase of reactive power can be observed as shown in Fig. 4 (f). As a result, the PCCB voltage of WPG₄ was maintained as presented in Fig. 4 (b).

In contrast to load bus 9, the voltage of load bus 7 located at the other side of the FWPS presented less magnitude drop as shown in Fig. 5 (a). Therefore, the generation current increase of WPG₁ was smaller than that of WPG₄, which is illustrated by the active power output of WPG₁ depicted in Fig. 5 (c). The dynamics of the capacitor voltage of WPG₁ is shown in Fig. 5 (g). The capacitor voltage of WPG₁ synchronized with that of WPG₄, which matches the analysis presented in Section II-B. Due to the capacitor voltage drop, the energy storage of WPG₁ increased its power output as illustrated in Fig. 5 (d). Meanwhile, the active power output of the SG

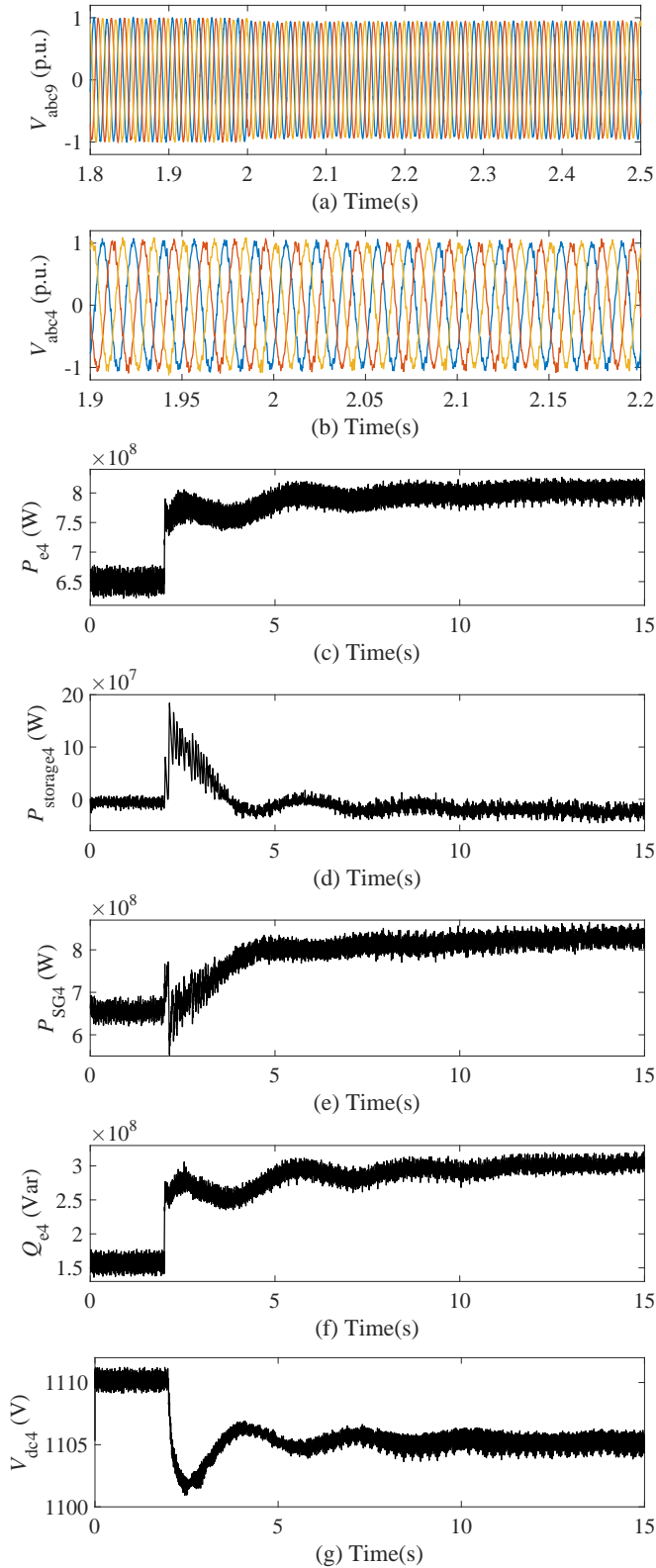


Fig. 4. Dynamics of WPG₄ obtained in the case where a 400 MW load was connected on load bus 9 at $t = 2$ s. ((a) Three-phase voltages measured on load bus 9 (b) Three-phase voltages measured on generator bus 4 (c) Active power output of WPG₄ (d) Power output of the energy storage of WPG₄ (e) Active power output of the SG of WPG₄ (f) Reactive power output of WPG₄ (g) Capacitor voltage of WPG₄)

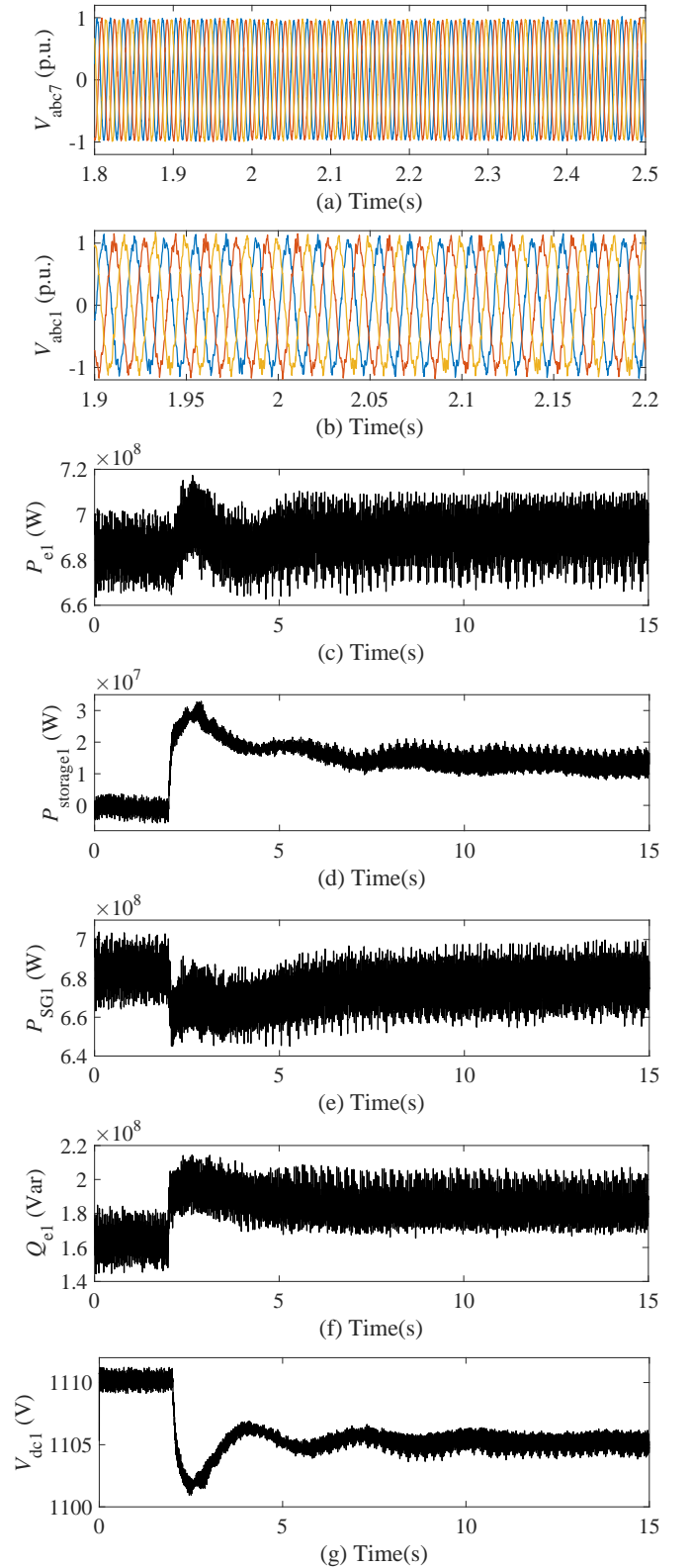


Fig. 5. Dynamics of WPG₁ obtained in the case where a 400 MW load was connected on load bus 9 at $t = 2$ s. ((a) Three-phase voltages measured on load bus 7 (b) Three-phase voltages measured on generator bus 1 (c) Active power output of WPG₁ (d) Power output of the energy storage of WPG₁ (e) Active power output of the SG of WPG₁ (f) Reactive power output of WPG₁ (g) Capacitor voltage of WPG₁)

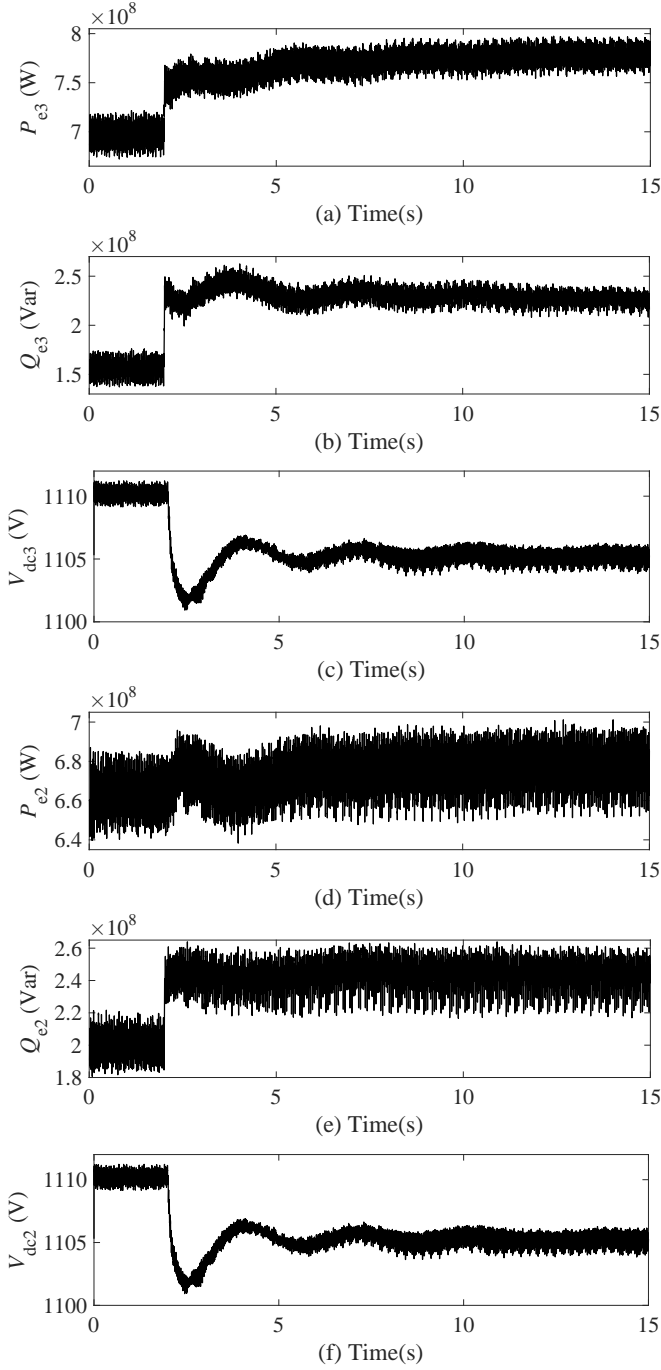


Fig. 6. Dynamics of WPG₂ and WPG₃ obtained in the case where a 400 MW load was connected on load bus 9 at $t = 2$ s. ((a) Active power output of WPG₃ (b) Reactive power output of WPG₃ (c) Capacitor voltage of WPG₃ (d) Active power output of WPG₂ (e) Reactive power output WPG₂ (f) Capacitor voltage of WPG₂)

of WPG₁ decreased slightly as depicted in Fig. 5 (e), in a coordinated manner with the energy storage dynamics such that P_{e1} presented in Fig. 5 (c) was obtained. The step up of the reactive power output of WPG₁ is presented in Fig. 5 (f). The three-phase voltages depicted in Fig. 5 (b) were measured on the PCCB of WPG₁.

WPG₃ and WPG₄ located on the same side of the FWPS, and they had presented similar dynamics. The active power and reactive power outputs of WPG₃ also showed step-wise increases as illustrated in Fig. 6 (a) and 6 (b), respectively.

Analogously, similar dynamics was observed on WPG₂ in comparison to that of WPG₁. The active and reactive power outputs of WPG₁ are illustrated in Fig. 6 (d) and 6 (e), respectively. The capacitor voltages of WPG₃ and WPG₂ synchronized with those of WPG₄ and WPG₁, which are illustrated by Fig. 6 (c) and 6 (f), respectively.

B. A Three-phase-to-ground Fault Occurred on the FWPS

A three-phase-to-ground fault occurred on the transmission line between bus 7 and bus 8 of the FWPS at $t = 2$ s. After 4 operating cycles, i.e. 66.7 ms, the fault transmission line was cut off by relay protection devices. Then the transmission line was switched on operation again at $t = 2.1667$ s.

Owing to the fault, the voltage of the transmission network of the FWPS dropped. The three-phase voltages measured on load bus 7 dropped to zero during the process when fault happened, which is shown in Fig. 7 (a). The voltage drop of the FWPS limited the active power transfer capability of the transmission network. As shown in Fig. 7 (c), the active power output of WPG₄ dropped to less than 400 MW. The capacitor voltage of WPG₄ then jumped to nearly 1130 V, as depicted in Fig. 7 (g). With the effort of the governor, the energy storage of WPG₄ output less power to the capacitor during the fault process as illustrated in Fig. 7 (d). The active power output of the SG of WPG₄ reduced as well, which is shown in Fig. 7 (e). With the exciter of the CVSC system, reactive power output of WPG₄ was increased to support its PCCB voltage. Consequently, three-phase voltages presented in Fig. 7 (b) were obtained on generator bus 4.

Other three WPGs presented similar dynamics with WPG₄. Fig. 8 (a), 8 (c), and 8 (e) present the dynamics of the active power outputs of WPG₁, WPG₂, and WPG₃, respectively. Active power outputs of all WPGs dropped when the fault happened. Capacitor voltages of WPGs varied in a synchronous manner, which are depicted in Fig. 8 (b), 8 (d), 8 (f), respectively.

V. CONCLUSIONS

This paper has proposed a CVSC system for the regulation of a FWPS. The inverters of WPGs are controlled with the equations of motion of capacitor voltages. With the CVSC system, the FWPS is enabled to operate in the same manner with conventional SG-based power systems.

According to the results of small-signal analysis, the FWPS controlled by the CVSC system is stable in the small. Low-frequency oscillatory modes are found in the rotational speed of wind turbines, and the design of oscillation damping controllers will be presented in our future work.

Simulation results, obtained in the case where a load increase occurred on the FWPS, have verified the capacitor voltage synchronizing performance of WPGs. Capacitors and energy storages of WPGs were able to provide inertial response to the load increase of the external power grid in a coordinated manner, which further enabled the SG of WPGs to offer inertial support to the drop of capacitor voltages. The governor with an active power-capacitor voltage droop characteristic ensured proper active power load sharing between WPGs in the FWPS.

Referring to the simulation results obtained in the case where a three-phase-to-ground fault occurred on the FWPS, the FWPS with the CVSC system is stable in the large. In contrast to the original four-generator two-area system, few low-frequency oscillations were observed in the dynamics of active power outputs and capacitor voltages of WPGs. The FWPS presented different transient characteristics in terms of high-frequency harmonic oscillations in both the tested cases, which is the inspiration for future works considering the harmonic stability of the FWPS.

REFERENCES

- [1] Global Wind Energy Council, "Gloable wind report: Annual market report 2015," http://www.gwec.net/wp-content/uploads/vip/GWEC-Global-Wind-2015-Report-April-2016_27_04.pdf.
- [2] BP Global, "BP statistical review of world energy June 2016," <http://www.bp.com/content/dam/bp/pdf/energy-economics/statistical-review-2016/bp-statistical-review-of-world-energy-2016-renewable-energy.pdf>.
- [3] L. A. de Souza Ribeiro, O. R. Saavedra, S. L. de Lima, and J. G. de Matos, "Isolated micro-grids with renewable hybrid generation: The case of lençóis island," *IEEE Trans. Sustain. Energy*, vol. 2, no. 1, pp. 1–11, Jan 2011.
- [4] Y. Liu, L. Jiang, Q. H. Wu, and X. X. Zhou, "Frequency control of DFIG based wind power penetrated power systems using switching angle controller and AGC," *IEEE Trans. Power Syst.*, vol. PP, no. 99, pp. 1–1, 2016.
- [5] L. Fan and Z. Miao, "Mitigating SSR using DFIG-based wind generation," *IEEE Trans. Sustain. Energy*, vol. 3, no. 3, pp. 349–358, July 2012.
- [6] J. H. Enslin, "Power system infrastructure: Do we face a complete power-electronics-based power system and energy-storage infrastructure?" *IEEE Power Electronics Magazine*, vol. 3, no. 2, pp. 42–45, June 2016.
- [7] M. C. Chandorkar, D. M. Divan, and R. Adapa, "Control of parallel connected inverters in standalone AC supply systems," *IEEE Trans. Ind. Appl.*, vol. 29, no. 1, pp. 136–143, Jan 1993.
- [8] J. M. Guerrero, L. G. de Vicuna, J. Matas, M. Castilla, and J. Miret, "A wireless controller to enhance dynamic performance of parallel inverters in distributed generation systems," *IEEE Trans. Power Electron.*, vol. 19, no. 5, pp. 1205–1213, Sept 2004.
- [9] N. Pogaku, M. Prodanovic, and T. C. Green, "Modeling, analysis and testing of autonomous operation of an inverter-based microgrid," *IEEE Trans. Power Electron.*, vol. 22, no. 2, pp. 613–625, March 2007.
- [10] Y. Shi, W. Wu, H. Wang, Y. Du, and J. Su, "The parallel multi-inverter system based on the voltage-type droop control method," *IEEE Journal of Emerging and Selected Topics in Power Electronics*, vol. 4, no. 4, pp. 1332–1341, Dec 2016.
- [11] M. N. Marwali, J.-W. Jung, and A. Keyhani, "Control of distributed generation systems - part II: Load sharing control," *IEEE Trans. Power Electron.*, vol. 19, no. 6, pp. 1551–1561, Nov 2004.
- [12] M. N. Marwali, J. W. Jung, and A. Keyhani, "Stability analysis of load sharing control for distributed generation systems," *IEEE Trans. Energy Convers.*, vol. 22, no. 3, pp. 737–745, Sept 2007.
- [13] R. Majumder, B. Chaudhuri, A. Ghosh, R. Majumder, G. Ledwich, and F. Zare, "Improvement of stability and load sharing in an autonomous microgrid using supplementary droop control loop," *IEEE Trans. Power Syst.*, vol. 25, no. 2, pp. 796–808, May 2010.
- [14] Y. Zhang and L. Xie, "A transient stability assessment framework in power electronic-interfaced distribution systems," *IEEE Trans. Power Syst.*, vol. 31, no. 6, pp. 5106–5114, Nov 2016.
- [15] J. M. Guerrero, L. Hang, and J. Uceda, "Control of distributed uninterruptible power supply systems," *IEEE Trans. Ind. Electron.*, vol. 55, no. 8, pp. 2845–2859, Aug 2008.
- [16] T. Caldognetto and P. Tenti, "Microgrids operation based on master-slave cooperative control," *IEEE Journal of Emerging and Selected Topics in Power Electronics*, vol. 2, no. 4, pp. 1081–1088, Dec 2014.
- [17] P. Kundur, N. J. Balu, and M. G. Lauby, *Power system stability and control*. McGraw-hill New York, 1994, vol. 7.
- [18] C.-M. Ong, *Dynamic simulation of electric machinery: using MATLAB/SIMULINK*. Prentice Hall PTR Upper Saddle River, NJ, 1998, vol. 5.
- [19] Y. Liu, Q. H. Wu, and X. X. Zhou, "Co-ordinated multiloop switching control of DFIG for resilience enhancement of wind power penetrated power systems," *IEEE Trans. Sustain. Energy*, vol. 7, no. 3, pp. 1089–1099, July 2016.

APPENDIX A NOMENCLATURE

ω_{ri}	Rotor speed of the SG of WPG _i
ω_{r_refi}	Reference of ω_{ri}
K_{p_pitch}	Proportional gain of the rotor speed control loop of wind turbine governors
β_i	Pitch angle of the turbine blades of WPG _i
P_{mei}	Power input to the capacitor of WPG _i
P_{me_refi}	Reference of P_{mei}
P_{ini}	Active power output of the SG of WPG _i
P_{in_refi}	The reference of P_{ini}
K_{p_comp}	Proportional gain of the proportional-integral (PI) controller of the power control loop of wind turbine governors
K_{i_comp}	Integral gain of the PI controller of the power control loop of wind turbine governors
$ \Psi_i $	Magnitude of the stator flux of the SG of WPG _i
$ \Psi_{i_ref} $	Reference of $ \Psi_i $
E_{fi}	Excitation voltage of the SG of WPG _i
K_{p_field}	Proportional gain of the PI controller of the exciter of SGs
K_{i_field}	Integral gain of the PI controller of the exciter of SGs
C	Capacity of the capacitor of WPGs
V_{dci}	Capacitor voltage of WPG _i
V_{dc_nom}	Nominal capacitor voltage of WPGs
K_{pg1}	Proportional gain of the governor of WPGs
K_{pg2}	Proportional gain of the governor of WPGs
K_{pg3}	Proportional gain of the governor of WPGs
I_{si}	Current injected by the energy storage of WPG _i
I_{s_refi}	Reference of I_{si}
L_{boost}	Inductance of the boost converter connected outside the rectifier
D_{duty}	Duty cycle of the boost converter of WPGs
$\Delta\theta_i$	Output of the phase angle control loop of the CVSC system of WPG _i
v'_{di}	d-axis reference voltage of the inverter of WPG _i
v'_{qi}	q-axis reference voltage of the inverter of WPG _i
ω_i	Rotational speed of the inverter voltage vector of WPG _i
m_i	Modulation index of the inverter of WPG _i
f_n	Nominal frequency of the FWPS
K_a	Gain of the phase angle control loop of the CVSC system
K_e	Gain of the exciter of the CVSC system
V_{ti}	Magnitude of the three-phase voltages measured on the PCCB of WPG _i
V_{t_refi}	Reference of V_{ti}
L_{filter}	Inductance of the RL filter connected outside the inverter of WPGs
R_{filter}	Resistance of the RL filter connected outside the inverter of WPGs
P_{mni}	Nominal mechanical power of WPG _i
P_{ni}	Nominal electrical power of WPG _i
V_n	Nominal line-to-line voltage of the stator of the SG of WPGs
V_{tn}	Nominal line-to-line voltage of the PCCB of WPGs
x_d	d-axis synchronous reactance of the SG of WPGs
x'_d	d-axis transient reactance of the SG of WPGs
x''_d	d-axis sub-transient reactance of the SG of WPGs
x_q	q-axis synchronous reactance of the SG of WPGs
x'_q	q-axis sub-transient reactance of the SG of WPGs
x_l	Stator leakage reactance of the SG of WPGs
T'_{d0}	d-axis transient open-circuit time constant of the SG of WPGs
T''_{d0}	d-axis sub-transient open-circuit time constant of the SG of WPGs
T'_{q0}	q-axis sub-transient open-circuit time constant of the SG of WPGs
R_s	Stator resistance of the SG of WPGs
p	Number of pole pairs of the SG of WPGs
Ψ_{di}	d-axis stator flux of the SG of WPG _i
Ψ'_{kqi}	q-axis transient flux of the damper windings of the SG of WPG _i
Ψ'_{kdi}	d-axis transient flux of the damper windings of the SG of WPG _i
ω_{ti}	Mechanical rotational speed of the wind turbine of WPG _i
Ψ'_{fi}	Transient flux of the field windings of the SG of WPG _i

APPENDIX B

PARAMETERS OF THE FULL-SCALE WPGs OF THE FWPS

TABLE II
PARAMETERS OF FULL-SCALE WPGs

Parameter	Value	Parameter	Value	Parameter	Value
P_{mni}	800 MW	P_n	889 MW	V_n	730 V
f_n	60 Hz	V_{tn}	575 V	L_{filter}	0.15 p.u.
R_{filter}	0.003 p.u.	V_{dc_nom}	1110 V	C	36 F
L_{boost}	0.0012 H	K_{p_pitch}	15	K_{p_comp}	1.5
K_{i_comp}	6	K_{p_field}	10	K_{i_field}	20
K_{pg1}	30	K_{pg2}	15	K_{pg3}	0.1
p	1	K_a	10	K_e	0.2
D_{duty}	0.19	x_d	1.305 p.u.	x'_d	0.296 p.u.
x''_d	0.252 p.u.	x_q	0.474 p.u.	x'_q	0.243 p.u.
x_l	0.18 p.u.	T'_{d0}	4.49 s	T''_{d0}	0.0681 s
T''_{q0}	0.0513	R_s	0.006 p.u.		



Yang Liu (CSEE: M'18, IEEE: M'18) received a B.E. degree and a Ph.D degree in Electrical Engineering from South China University of Technology (SCUT), Guangzhou, China, in 2012 and 2017, respectively. He is currently an Associate Professor in the School of Electric Power Engineering, SCUT. His research interests include the areas of power system stability analysis and control, control of wind power generation systems, and nonlinear control theory. He has authored or co-authored more than 30 peer-reviewed SCI journal papers, and a monograph published by Springer Nature named as "Switching Control of Large-Scale Complex Power Systems-Theory and Applications".

published by Springer Nature named as "Switching Control of Large-Scale Complex Power Systems-Theory and Applications".

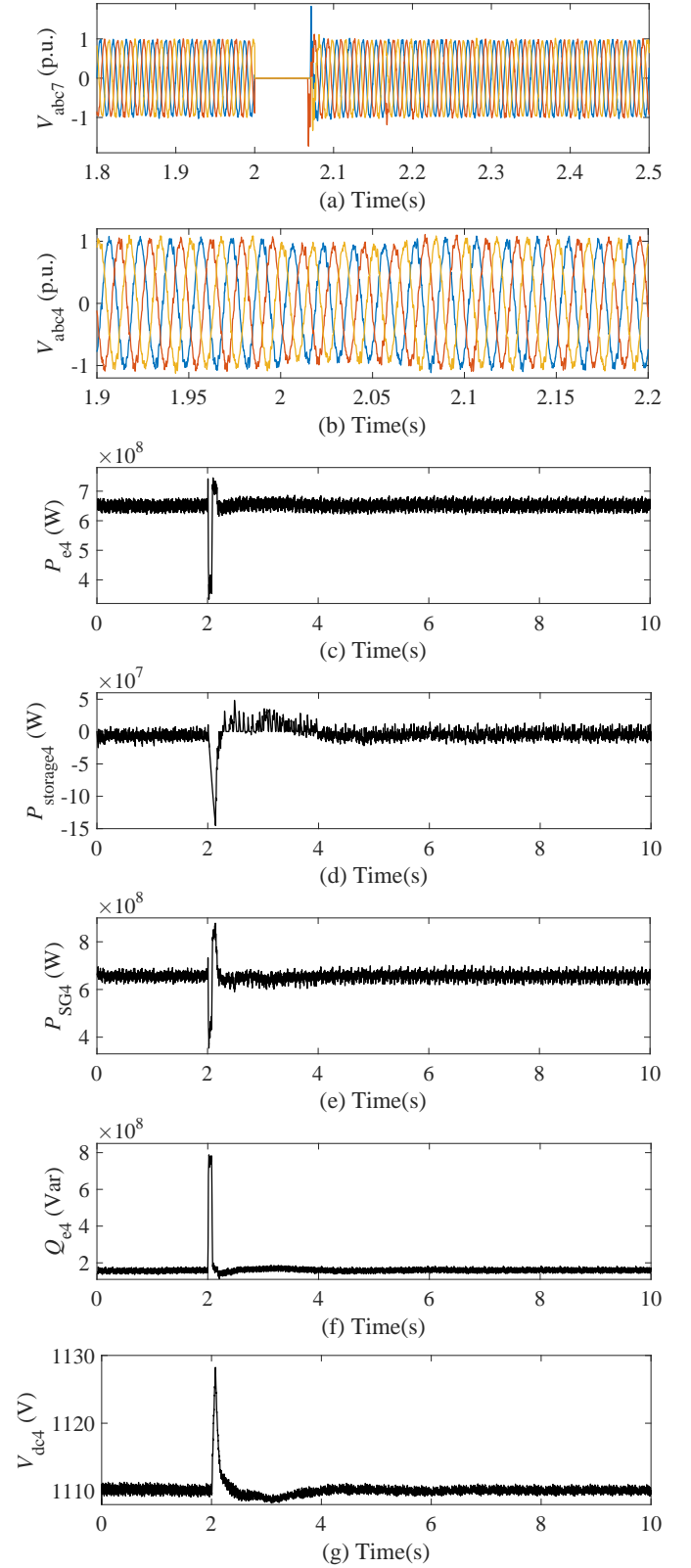


Fig. 7. Dynamics of WPG₄ obtained in the case where a three-phase-to-ground fault occurred on the transmission line between bus 7 and bus 8 at $t = 2$ s. ((a) Three-phase voltages measured on load bus 7 (b) Three-phase voltages measured on generator bus 4 (c) Active power output of WPG₄ (d) Power output of the energy storage of WPG₄ (e) Active power output of the SG of WPG₄ (f) Reactive power output of WPG₄ (g) Capacitor voltage of WPG₄)

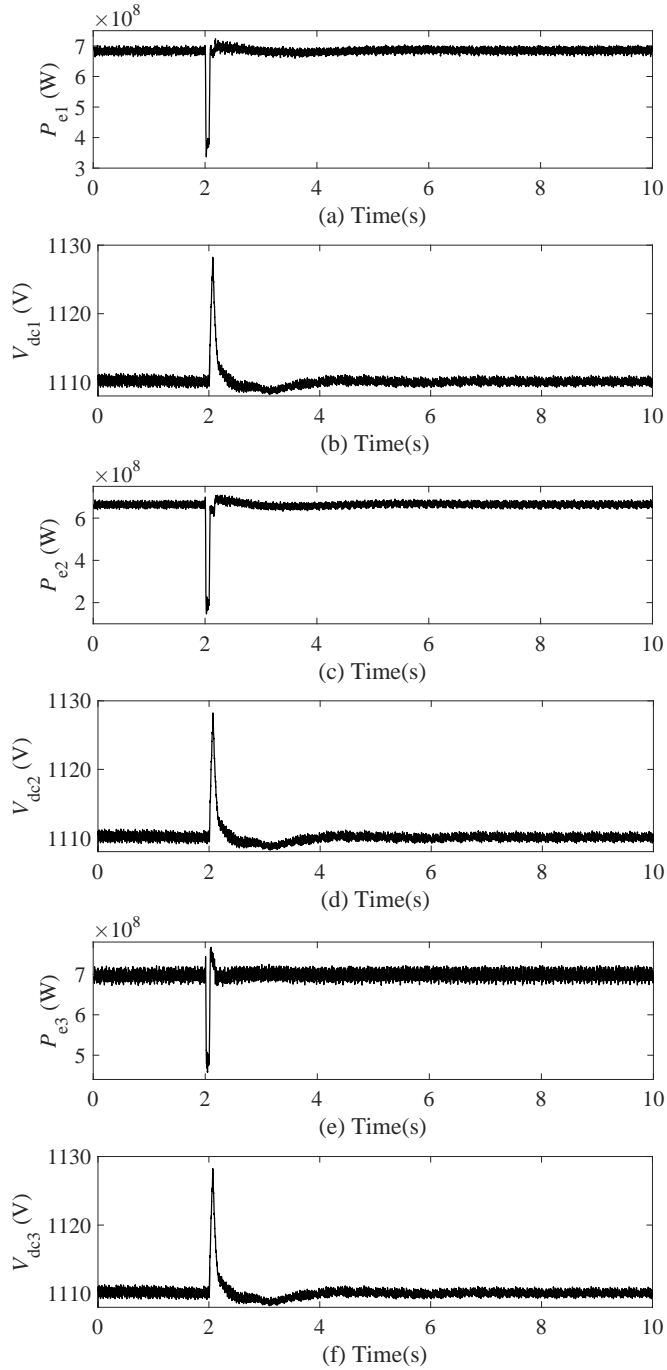


Fig. 8. Dynamics of WPG₁, WPG₂, and WPG₃ obtained in the case where a three-phase-to-ground fault occurred on the transmission line between bus 7 and bus 8 at $t = 2$ s. ((a) Active power output of WPG₁ (b) Capacitor voltage of WPG₁ (c) Active power output of WPG₂ (d) Capacitor voltage of WPG₂ (e) Active power output of WPG₃ (f) Capacitor voltage of WPG₃)